

## Spatial and temporal Hurst exponent variability of rainfall series based on the climatological distribution in a semiarid region in Mexico

Alvaro Alberto LÓPEZ-LAMBRAÑO\*<sup>1,2</sup>, Carlos FUENTES<sup>3</sup>, Alvaro Alberto LÓPEZ-RAMOS<sup>4</sup>,  
Jorge MATA-RAMÍREZ<sup>1</sup> and Mariangela LÓPEZ-LAMBRAÑO<sup>5</sup>

<sup>1</sup> *Facultad de Ingeniería, Arquitectura y Diseño, Universidad Autónoma de Baja California, km 103 carretera Tijuana-Ensenada, 22860 Ensenada, Baja California, México.*

<sup>2</sup> *HIDRUS, Querétaro, México.*

<sup>3</sup> *Instituto Mexicano de Tecnología del Agua, Paseo Cuauhnahuac 8532, Col. Progreso, 62550 Jiutepec, Morelos, México.*

<sup>4</sup> *Facultad de Ingeniería Civil, Escuela de Ingenierías y Arquitectura, Universidad Pontificia Bolivariana-Seccional Montería, Cra 6 Núm. 97A-99, Montería, Córdoba, Colombia.*

<sup>5</sup> *Universidad del Norte, km 5 vía Puerto Colombia, Barranquilla, Colombia.*

\*Corresponding author; email: altoti@gmail.com

Received: September 21, 2016; accepted: March 14, 2018

### RESUMEN

Se realiza un análisis fractal de los eventos de lluvia registrados en Baja California, México, una región semiárida que presenta amplia variabilidad climatológica. Se utilizan series de precipitación de 92 estaciones climatológicas con longitudes de registro mayores a 30 años. Se determinan patrones y características en las series de precipitaciones a partir de valores espaciales y temporales del exponente de Hurst, así como su relación con la temperatura y precipitación media anual, altitud y distribución climatológica. Se emplean con éxito los métodos de rango reescalado, conteo de cajas y análisis multifractal de fluctuación sin tendencia, lo cual permite obtener el valor promedio del exponente de Hurst para diferentes escalas de tiempo. Los datos muestran que la serie de precipitación diaria tienden a presentar un patrón persistente; además, los valores del exponente de Hurst se relacionan con el tipo de clima, la altitud, el régimen de lluvias y la temperatura en la zona de estudio. El análisis del exponente de Hurst para diferentes escalas de tiempo evidencia que dicho exponente aumenta a medida que la escala de tiempo en consideración es menor; por lo tanto, la persistencia de la serie se hace más fuerte. Por otra parte, se puede confirmar que la teoría fractal permite analizar el comportamiento de una variable climática, en este caso, la precipitación.

### ABSTRACT

A fractal analysis from rainfall events registered in a semiarid region was carried out. The analysis was executed for Baja California, Mexico, a region that presents a high climatological variability. Rainfall data from 92 climate stations distributed along the region of study with at least 30 years of records were used. By studying the rainfall series patterns, the Hurst exponent values were obtained (both spatial and temporal) as well as their relation with the variables for annual average temperature, annual average rainfall, altitude and climatological distribution. The rescaled range method, box counting method, and multifractal detrended fluctuation analysis were successfully applied, having as a result the average value of the Hurst exponent for different time scales. Data showed that the daily rainfall series tend to present a persistent pattern; besides, the Hurst exponent values ( $H_u$ ) were related to the type of climate, altitude, rainfall regime, and temperature of the studied area. The analysis of the Hurst exponent for different time scales showed that, at a smaller time

scale, the Hurst value tends to increase; thus, the series present a stronger persistent behavior. Moreover, it can be confirmed that the fractal theory methodology allows analyzing the behavior of a climate variable, in this case rainfall.

**Keywords:** Time scale, fractal dimension, climate variable.

## 1. Introduction

The aim of this research is to analyze the fractal behavior of rainfall events in a semiarid region located in Baja California, northwestern Mexico. Two analyses were performed to: (1) find a relation with climatological distribution, altitude, average temperature and average annual rainfall, and (2) compare different scales for the same time series. In order to achieve this goal, 92 climate stations with at least 30 yrs of records were analyzed; subsequently, using the Hurst exponents, a spatial and temporal analysis was carried out in order to compare it with the previously mentioned variables. The results could help analyzing the effects of climate change in this region.

It is well known that rainfall, being a random variable and part of a complex and chaotic system (Xu et al., 2015), evolves during time and space and exhibits extreme variability (Brunsell, 2010; Gires et al., 2014), as well as temporal trends (Shi et al., 2014), which also implies that these two dimensions are not mutually independent. It has been also found that the evolution ratio of rainfall is invariant through time and space in a dynamic scale, and that over wide ranges, atmospheric spatial variability can be well described (Pinel et al., 2014). Rainfall events are very erratic at short and large temporal and spatial scales (Millan et al., 2011). According to Zhang et al. (2013), rainfall extreme events have become more frequent and intense under global warming conditions, causing an increase in the number of days with extreme rainfall events; therefore studying the spatial correlation structure exhibited by rainfall measurements can provide useful results for understanding the effects produced by the interaction between meteorological patterns (Sirangelo and Ferrari, 2014). The statistical structure dependence of rainfall in space and time can be analyzed with a single parameter that studies its persistence (Venugopal et al., 1999). A research conducted in India proved that regional climatological models were

not capable of adequately predicting local weather since they use average values; therefore, models that study the internal structure of the random variable are required (Rangajaran and Sant, 2004). The foundation of this statement is that extremely variable fields, such as rainfall, involve multiple scales and dimensions, being these two characteristics present in intense regions (Lovejoy et al., 1987). It has been confirmed that rainfall is a part of many factors involved in climate change which are characterized by persistence in the long term (Fluegeman and Snow, 1989). Hydrological data sets, such as rainfall, are constituted of complex fractal geometry which is complicated to represent using classical stochastic methods (Huai-Hsien et al., 2013). However, trying to study a single random variable at different scales turns out to be very complex, along with the fact that autoregressive methods can produce certain errors (Svanidze, 1980); hence, a new and revolutionary approach has emerged (Sivakumar, 2000) that has proven to be much more effective than classical autoregressive methods (Caballero et al., 2002; Nunes et al., 2011; Akbari and Friedel, 2014).

Mandelbrot (1967) introduced the concept of a fractal in terms of self-similar statistic; this concept revolves around the idea that the shape of an object does not define its size. Mandelbrot defined fractals as objects that possess a similar appearance when observed at different scales, having details even at small arbitrary scales; such fractals are too complex to be studied under Euclidian geometry laws. Fractals allow the generation of very complex structures through groups which can be applied to virtually any research of interest (Lovejoy and Mandelbrot, 1984). Fractals are assigned non-integer-value dimensions resulting in successful modeling of many natural phenomena. One of the most important developed approaches is the representation of time series as curves with dimensions between 1 and 2. Usually, two methods are used to determine the fractal dimension of these phenomena: the rescaled range analysis (R/S)

(Mandelbrot, 1972) and the box counting method (Falconer, 1990; Breslin and Belward, 1999). Other methods such as the wavelet transform method are applied as well (Yan-Fang, 2013).

In order to obtain the fractal dimension, the rescaled range method divides the range of partial sums of deviations from the mean of a time series by the standard deviation (Hurst, 1951, 1956). The box counting method considers variable fields such as rainfall, which involves multiple scales and dimensions that characterize intense regions (Lovejoy et al., 1987).

Now, it is well known that rainfall events are highly important, not only for scientific purposes but for all the possible imaginable ramifications. However, this research field changed drastically with the contributions of Hurst and Mandelbrot, as well as many studies performed all over the world, which enforced the relation between this variable and a fractal behavior (Turcotte, 1994; Peters et al., 2002).

For this study, we have chosen to work with fractals instead of methods involving probability, given that dynamic systems display in nature self-similarity and space-time fluctuations on their behavior on all scales, indicating correlation on a large range; therefore, normal and average distribution, as well as standard deviation approaches cannot be used to properly describe and quantify fractal sets (Selvam, 2010). Fractals behave in a different dimension than the Euclidian dimension counterparts, known as fractal dimension ( $D_f$ ), which is usually smaller than the Euclidian dimensions. The application of fractals to hydrology is important since the current models are too simple to approach the behavior of rainfall events. Decades ago, fractals were considered geometric monsters; however, to give an example, it is now known that they perfectly describe rainfall and pluvial discharge (Schertzer et al., 2010). It is also important to mention that the general trend analysis for rainfall events is vital for the purpose of identifying changes (Selvi and Selvaraj, 2011). Usually, fractal geometry studies, applied to rainfall events, are focused on estimating the fractal dimension. Several researches have been carried out all over the world. In Italy, a comparison between the fractal dimensions of rainfall events detected through radar/satellite methodologies was conducted (Capecchi et al., 2012), as well as an evaluation of rainfall events at different

climatological stations, finding a relation in specific time intervals. It was observed that the fractal dimension describes the magnitude of rainfall events in a more realistic way compared to the traditional methods, discovering that the more isolated the particles of rain are, the lower the fractal dimension obtained will be (Mazzarella, 1999).

Furthermore, there are certain methodologies in fractal studies, e.g., models can be created so they can reproduce certain types of a self-similar behavior observed in rainfall (Troutman and Over, 2001). Fractals applied to hydrology have a huge field of application. For example, fractal methods have proven to be very useful in the analysis and synthesis of rain fields. The fractal model is presented in order to simulate rain fields using an additive-iterative process in the logarithmic domain, resulting in monofractal fields with a spectral density exponent and a fractal dimension (Callaghan and Villar, 2007). They also allow the comparison between various methods in order to verify their efficiency, which is the case of a comparison made between two methods in order to analyze 27 convective storms in United States, showing that both methods were very efficient and yielded very consistent structural fields (Tao and Barros, 2010).

In the case of fractal studies with rainfall approaches, it has been found that the Hurst exponent value is influenced by the altitude of the studied region. A research in Zacatecas, Mexico, showed that altitude causes a negative influence on the Hurst exponent, i.e., climatological stations located at higher altitudes generate an anti-persistent behavior (Velásquez et al., 2013). Furthermore, there have been many studies involving rainfall and fractals, the most noted being an application of the R/S to study the fractal properties of rainfall events from 1921-2010, resulting in time series that showed fractal behavior. The fractal dimension was similar to the one obtained in previous studies, which suggests that the majority of these series showed persistence in the long term (Beran, 1994), which proves that rainfall is a phenomenon that can be characterized through its fractal dimension (Amaro et al., 2004). A large scale project in South America and Europe was conducted in order to compare fractal dimensions between rainfall time series using data from over 30 yrs in order to calculate their dependence in time.

Both places found tendencies at different frequencies, achieving very precise results (Kalauzi et al., 2009). Other interesting approaches were those conducted in China, where flood time series were analyzed using fractals; the sequence was reproduced and it helped to prevent an extreme event many years later by using the Hurst exponent (Chang and Wang, 1999); in Ecuador, multifractal analysis of climatic variables including rainfall events (Millan et al., 2008) and a multifractal study regarding meteorological dynamics (Millan et al., 2010) were conducted; in Tokyo, Japan, where rainfall events were studied using multifractals (Pathirana et al., 2001); and in France, where the effect of considering zero values in rainfall series was analyzed through fractal geometry (Gires et al., 2012), which according to Verrier et al. (2010) influences the results.

Another important application was conducted to identify the scalar behavior of time series using a method called multifractal detrended fluctuation analysis, which helped to understand fractals and provided a statistic behavior approach (Ge and Yee, 2013); furthermore, multifractal analysis has been found to be a useful tool to establish intensity fluctuations of atmospheric data (Arizabalo et al., 2015). A rain field research, using a spectral analysis in Iowa, was performed as well (Pavlopuolos and Krajewski, 2014). Finally, it is important to mention the annual rainfall events in Spain as an important breakthrough: in 10 stations which were studied from 1901-1989, the fractality of rainfall was proven with a fractal dimension of 1.32, a very similar value to macrometeorological records (Oñate, 1997). It can be said that fractals' impact on science has been possible due to the Hurst theory. Moreover, it can be concluded that fractals allow the creation of complex structures and, in particular for hydrology, the ability to model rainfall events (Lovejoy and Mandelbrot, 1984).

## 2. Data and methods

The area of study is Baja California, Mexico, comprised between the coordinates 32.713° N, 114.723° W; 32.527° N, 117.141° W; 28.095° N, 115.364° W; and 27.994° N, 112.799° W. This region in the northwest of Mexico possesses high climatological and physiographical variability, so we required using maps

that allowed us to visualize both climatological and physiographical characteristics. For the purpose of this study, daily rainfall data from 92 climate stations were used. A map of climate distribution according to the Köppen classification (Köppen, 1918) was obtained from the Instituto Nacional de Estadística y Geografía (National Institute of Statistics and Geography, INEGI); furthermore, the studied climate stations were georeferenced on the map (Fig. 1).

### 2.1 Spline interpolation method

The maps for average annual rainfall (Fig. 2a), average daily temperature (Fig. 2b), and altitude above sea level (Fig. 2c) were obtained through a spatial interpolation using the spline method based on the climatological information provided by each station. Among several methods that were considered, such as the inverse distancing weighing method, the kriging method, and the natural neighbor interpolation method, the spline interpolation method was selected as the best. The result, although not shown in this paper, proves that for this case, the spline method presents the smallest mean square error. The average annual rainfall (Fig. 2a) was obtained by calculating the average annual value of rainfall for each station, and then proceeding to a spatial interpolation. The average daily temperature map (Fig. 2b) and the altitude above sea level maps (Fig. 2c) were obtained in a similar way by interpolating their respective variables.

According to Hazenwinkel (2001), spline is a form of interpolation where the interpolator is a special type of polynomial called spline. This is very useful since the interpolation error can be smaller using this method. Also, this method is based on putting a curve through a determined number of points. The mathematical approach of this model is based on  $n + 1$  nodes  $(x_i, y_i)$   $i = 0, 1, \dots, n$  and interpolate between pairs of nodes  $(x_{i-1}, y_{i-1})$  and  $(x_i, y_i)$  with polynomials  $y = q_i(x)$ ,  $i = 1, 2, \dots, n$  where the curvature of the curve

$$Y = f(x) \quad (1)$$

Is:

$$k = \frac{y''}{(1 + y'^2)^{3/2}} \quad (2)$$

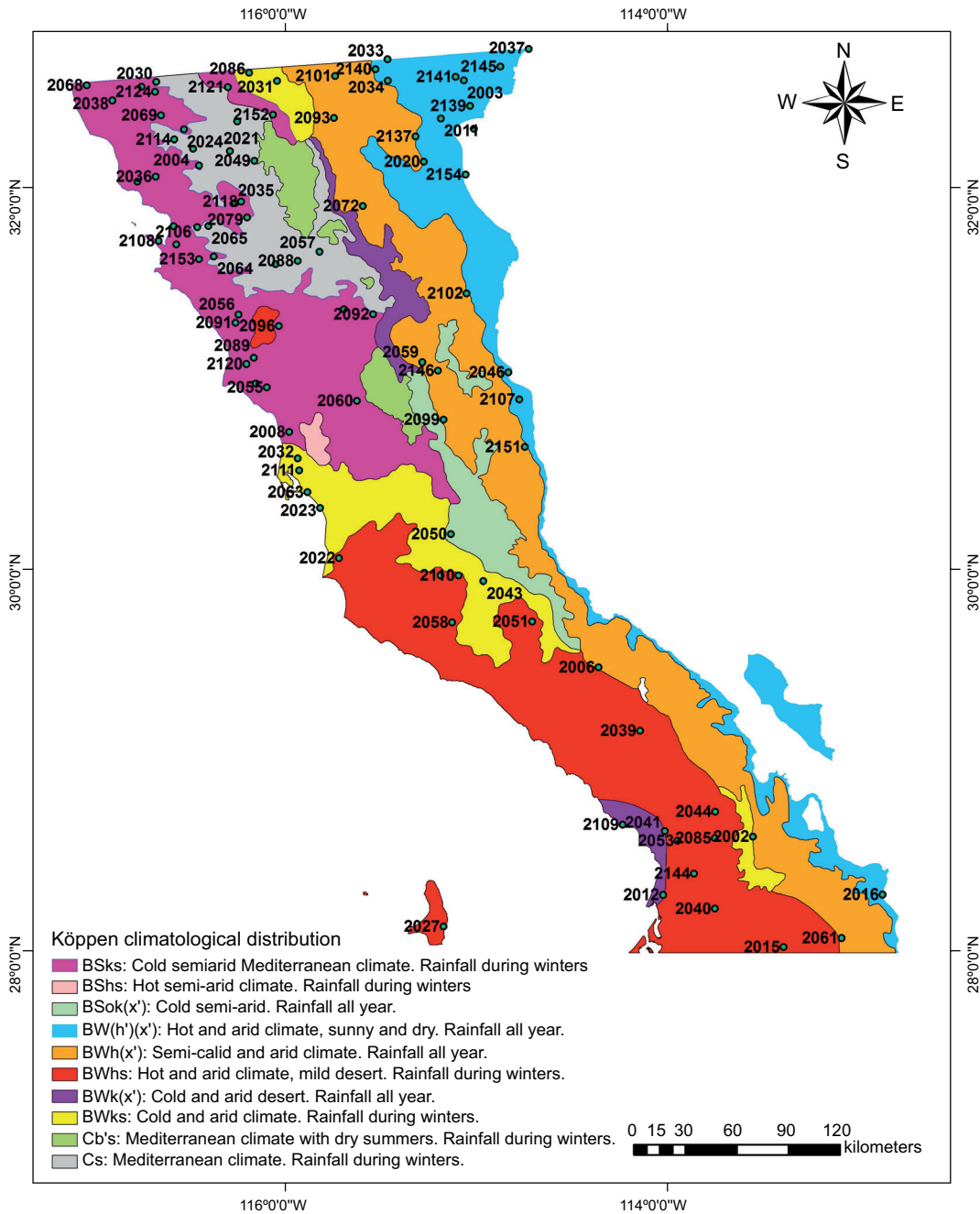


Fig 1. Climatological distribution of Baja California, Mexico, according to the Köppen classification.

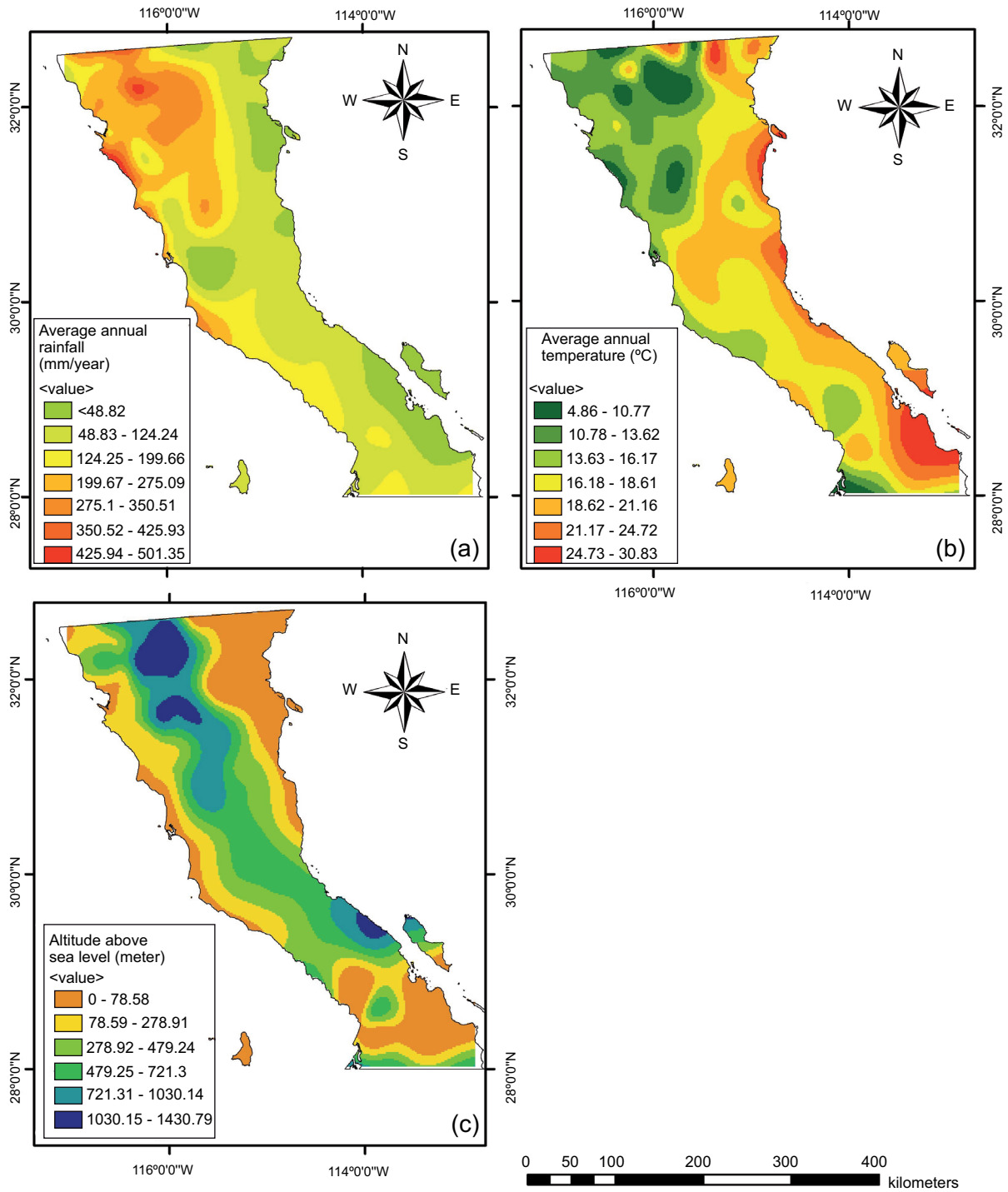


Fig. 2. Climatological and physiographic variables in Baja California. (a) Average annual rainfall (mm/yr). (b) Average annual temperature (°C). (c) Altitude above sea level (m).

Therefore, the spline will minimize the bend, so  $y'$  as well as  $y''$  will be continuous in the nodes:

$$q'_i(x_i) = q'_{i+1}(x_i) \tag{3}$$

$$q''_i(x_i) = q''_{i+1}(x_i) \tag{4}$$

for all values of  $i$ ,  $1 \leq i \leq n-1$ .

The next step is the fractal analysis of the data. To do so, 92 climatological stations with 30 yrs of daily rainfall data records were analyzed. In order to obtain the previously mentioned data, the Rapid Climatological Information Extractor (ERIC III) software and CLImate COMputing project (CLICOM), both of which include daily national climate data.

For the purpose of this research, the use of three different methods for calculating the Hurst exponent of each time series is required in order to get an average value that reflects a higher precision and reliability in the results. These three methods were the rescaled range analysis (R/S), the box counting method, and the multifractal detrended fluctuation analysis (MF-DFA) algorithm.

A determinant factor when selecting the method to apply was the number of available input parameters, meaning that the model would be more complex if it had a greater number of parameters. The considered methods in the present study are easy to apply and have been widely referenced in the recent literature (López-Lambrano et al., 2017). Also, the methods we applied allow detecting non-periodic cycles and long term correlations in random processes; furthermore, they are not influenced by the occurrence of probable lineal tendencies presented in series, and they manage to detect long-range correlations in non-stationary time series just as the MF-DFA does.

By employing the Benoit software, Hurst exponent values were obtained for both the R/S and the box counting methods. The computational algorithm for MF-DFA was programmed following the considerations established by Movahed et al. (2006).

### 2.2 Rescaled range method (R/S)

An alternative approach to the correlation quantification in a time series analysis was developed by Hurst

(1951, 1956), who spent his entire life studying the hydrology of the Nile river, particularly on droughts and floods. Hurst considered the river's flow as a time series and determined storage limits. Based on his studies, he empirically introduced the concept of R/S. Considering a time series, the summation of time series relative to their average value is:

$$y_n = \sum_{i=1}^n (y_i - \bar{y}_N) = \left( \sum_{i=1}^n y_i \right) - n\bar{y}_N \tag{5}$$

where the range is defined by

$$R_N = (y_n)_{\max} - (y_n)_{\min} \tag{6}$$

with

$$S_N = \sigma_N \tag{7}$$

where  $\bar{y}_N$  and  $\sigma_N$  are the mean and standard deviations of all the  $N$  values in the time series  $y_n$ . From the previous equations, a value  $(R_N/S_N)$  is obtained for the time series  $y_n$ . We substitute  $\tau$  by  $N$  in equations 5 to 7. The Hurst exponent ( $H_u$ ), is obtained as:

$$\left( \frac{R_\tau}{S_\tau} \right)_{av} = \left( \frac{\tau}{2} \right)^{H_u} \tag{8}$$

The rescaled range  $R/S(w)$  is defined as:

$$R/S(w) = \left\langle \frac{R(w)}{S(w)} \right\rangle \tag{9}$$

where  $w$  is the window width and the symbols  $\langle \rangle$  represent the average values of a number of values of  $R(w)$ . The foundation of the method is that, based on the self-affinity, it can be expected that

$$R/S(w) = w^{H_u} \tag{10}$$

In practice, for a determined value of  $w$ , a time series is subdivided by a number of intervals of width  $w$ , then  $R(w)$  and  $S(w)$  are calculated for each one, and  $R/S(w)$  as the average ratio  $R(w)/S(w)$ . This procedure is repeated for a determined number of window widths, and the logarithms of  $R/S(w)$  are plotted against the logarithms of  $w$ . If the set has self-affinity, then the plot will follow a straight line whose slope is equal to the Hurst exponent  $H_u$ . The fractal dimension of the set can be calculated from the Hurst exponent-fractal dimension relation:

$$D_{rs} = 2 - H_u \quad (11)$$

where  $D_{rs}$  denotes the fractal dimension calculated by the rescaled range method.

### 2.3 Box counting method

According to Peñate et. al. (2013), the box counting method is based on dividing the space of observation (the time interval  $T$ ) into  $n$  non-overlapping segments of characteristic size  $s$ , so that  $s = T/n$  for  $n = 2, 3, 4, \dots$ , and computing the number  $N(s)$  of intervals of length  $s$  occupied by events. If the distribution of events has a fractal structure, then the relationship  $N(s) = Cs^D$  prevails. The fractal or box counting dimension  $D_f$  is estimated from the slope  $D$  of the regression line of  $\log(N(s))$  on  $\log(s)$ . This parameter  $D_f = |D|$  describes the strength of the events and can measure the phenomenon's nature, since it quantifies the scale-invariant clustering of the time series. Clustering increases when  $D$  approaches 0. Hence, the smallest fractal dimensions correspond to clusters formed by events that occur sparsely. If  $D$  is close to 1, the events are randomly spaced in time. To sum up, the box counting method uses boxes to cover an object in order to find the fractal dimension. The signal is partitioned into boxes of various sizes and the amount of non-empty squares is counted. A log-log plot of the number of boxes vs. the size of the boxes is done. The box dimension is defined by the exponent  $D_b$  in the relation

$$N(s) \equiv \frac{1}{s^{D_b}} \quad (12)$$

where  $N(s)$  is the number of boxes with linear size  $s$  needed to cover the set of points distributed on a bidimensional plane. A number of boxes, proportional to a  $1/s$ , are needed to cover the set of points on a line; proportional to  $1/s^2$ , to cover a set of points on a plane, etc.

In theory, for each box size, the grid should be configured in such a way that the minimum number of boxes is occupied. This can be achieved by rotating the grid for each box size in  $90^\circ$  and plotting the minimum value of  $N(d)$ .

### 2.4 Multifractal detrended fluctuation analysis

According to Yuval and Broday (2010), Movahed et al. (2006) and Kantelhardt et al. (2002), the

modified multifractal DFA (MF-DFA) procedure consists of five steps. Suppose that  $x_k$  is a series of length  $N$ , and that this series is of compact support, i.e.,  $x_k = 0$ , only for an insignificant fraction of the values.

Step 1. Determination of the profile:

$$Y(i) \equiv \sum_{k=1}^i [x_k - \langle x \rangle], \quad i=1, \dots, N. \quad (13)$$

Subtraction of the mean  $\langle x \rangle$  is not compulsory, since it would be eliminated by the later detrending in the third step.

Step 2. Division of the profile  $Y(i)$  into  $N_s = \text{int}(N/s)$  non-overlapping segments of equal lengths  $s$ . Since the length  $N$  of the series is often not a multiple of the considered timescale  $s$ , a short part at the end of the profile may remain. In order to disregard this part of the series, the same procedure is repeated starting from the opposite end. Thereby,  $2N_s$  segments are obtained altogether.

Step 3. Calculation of the local trend for each of the  $2N_s$  segments by a least square fit of the series. Then the variance should be determined:

$$F^2(s, v) \equiv \frac{1}{s} \sum_{i=1}^s \{Y[(v-1)s+i] - y_v(i)\}^2 \quad (14)$$

for each segment  $v$ ,  $v = 1, \dots, N_s$ , and:

$$F^2(s, v) \equiv \frac{1}{s} \sum_{i=1}^s \{Y[N - (v - N_s)s + i] - y_v(i)\}^2 \quad (15)$$

for  $v = N_s + 1, \dots, 2N_s$ . Here  $y_v(i)$  is the fitting polynomial in segment  $v$ . Linear, quadratic, cubic or higher order polynomials can be used in the fitting procedure. Since the detrending of the time series is done by the subtraction of the polynomial fits from the profile, different order DFA differ in their capability of eliminating trends in the series.

Step 4. Average over all segments to obtain the  $q$ th-order fluctuation function, defined as

$$F_q(s) \equiv \left\{ \frac{1}{2N_s} \sum_{v=1}^{2N_s} [F^2(s, v)]^{q/2} \right\}^{1/q} \quad (16)$$

where, in general, the index variable  $q$  can take any real value except zero. For  $q = 2$ , the standard DFA procedure is retrieved. Generally, we are interested in how the generalized  $q$ -dependent fluctuation functions  $F_q(s)$  depend on timescale  $s$  for different values of  $q$ . Hence, we must repeat steps 2, 3 and 4 for several timescales  $s$ . It is apparent that  $F_q(s)$  will

increase while  $s$  increases. Of course  $F_q(s)$  depends on the DFA order  $m$ . By construction,  $F_q(s)$  is only defined for  $s \geq m + 2$ .

Step 5. Determination of the scaling behavior of the fluctuation functions by analyzing log-log plots of  $F_q(s)$  versus  $s$  for each value of  $q$ . If the series  $x_i$  are correlated by the long-range power-law,  $F_q(s)$  increases, for large values of  $s$ , as a power law:

$$F_q(s) : s^{h(q)} \quad (17)$$

In general, the exponent  $h(q)$  may depend on  $q$ . The exponent  $h(2)$  is identical to the well-known Hurst exponent ( $H_u$ ).

A decimal fraction—as fractal dimension—allows describing fractal geometry as well as the heterogeneity of irregular sets, which enables us to record any lost data if traditional geometry representations were applied. A relationship between the fractal dimension and the Hurst coefficient for the used fractal methods is defined by  $2H + 1 = 5 - 2D_{rs}$ . If we solve the equation for  $D_{rs}$  we obtain Eq. (11). This idea establishes a robust analysis, since long-term persistence conditions can be assessed, non-periodic cycles can be detected, and long-term random processes can be established. When we encounter a fractal dimension which is close to the unit, we can confirm highly persistent series and a limited variation.

### 2.5 Fractal considerations

In order to estimate the Hurst exponent for the proposed time series, the following considerations and time scales were taken into account:

1. Hurst exponent values calculated from the analysis of the complete time series. In order to estimate the  $H_u$  value for this first consideration, the three methods were employed. Then the three obtained values were averaged.
2. Hurst exponent values calculated from the analysis of a time series in periods of 25 yrs. In this matter we followed the same procedure mentioned above. However, the time series was partitioned into two periods of 25 yrs.
3. Hurst exponent values calculated from the analysis of a time series in periods of 10 yrs.
4. Hurst exponent values calculated from the analysis of a time series in periods of 5 yrs. For

considerations three and four, the procedure was done using the approach proposed in point two.

5. After obtaining the Hurst exponents from the climate stations, a spline interpolation was conducted; additionally, spatial distribution maps (presented below) were generated where the Hurst exponent values were interpolated based on the average results for each climate station. The maps for the complete time series (Fig. 3a) and for the time scales of 25 (Fig. 3b), 10 (Fig. 3c), and 5 yrs (Fig. 3d) were generated.

### 3. Results and discussion

Maps for Köppen's climatological classification (Fig. 1), annual pluvial regime (Fig. 2a), average annual temperature (Fig. 2b) and meters above sea level (Fig. 2c) were generated from the data obtained from the 92 climate stations with more than 30 yrs of daily rainfall records (Tables I and II).

Considering the classification of climates in Baja California (Fig. 1), it can be seen that the values of the Hurst exponent ( $H_u$ ) may be associated with the climatological conditions of the analyzed region, meaning that climates with daily rainfall regime during winter (BSKS, Cs, BWks and BWhs) obtain lower  $H_u$  values (between 0.4 and 0.6), corresponding to persistent and anti-persistent behaviors. Compared to other studies, our results are similar to those obtained by Gutiérrez et al. (2006) in Australia, with BWhs climate and  $H_u$  values between 0.4 and 0.56; however, they differ from the results obtained by Yuval and Broday (2010) in Israel with BWks and Cs climates, and  $H_u$  values of 0.7, as well as Zhou et al. (2005) in Botswana with climate BWks and  $H_u$  values from 0.55 to 0.92. For climates with daily rainfall regime throughout the year—BWk(x'), BW(h')(x'), BWk(x') and BSok(x')—the obtained values are ranging between 0.57 and 0.86, meaning that there is a persistent behavior which is similar to the result obtained by Rehman (2009) in Saudi Arabia with BWk(x') climate and  $H_u$  values between 0.59 and 0.71. Since climates with rainfall throughout the year are predominant in Baja California, most of the registered precipitation events show a persistent behavior over time. Climates that have very arid and semi-arid conditions with daily rainfall throughout the year BWk(x') and climates with very arid and

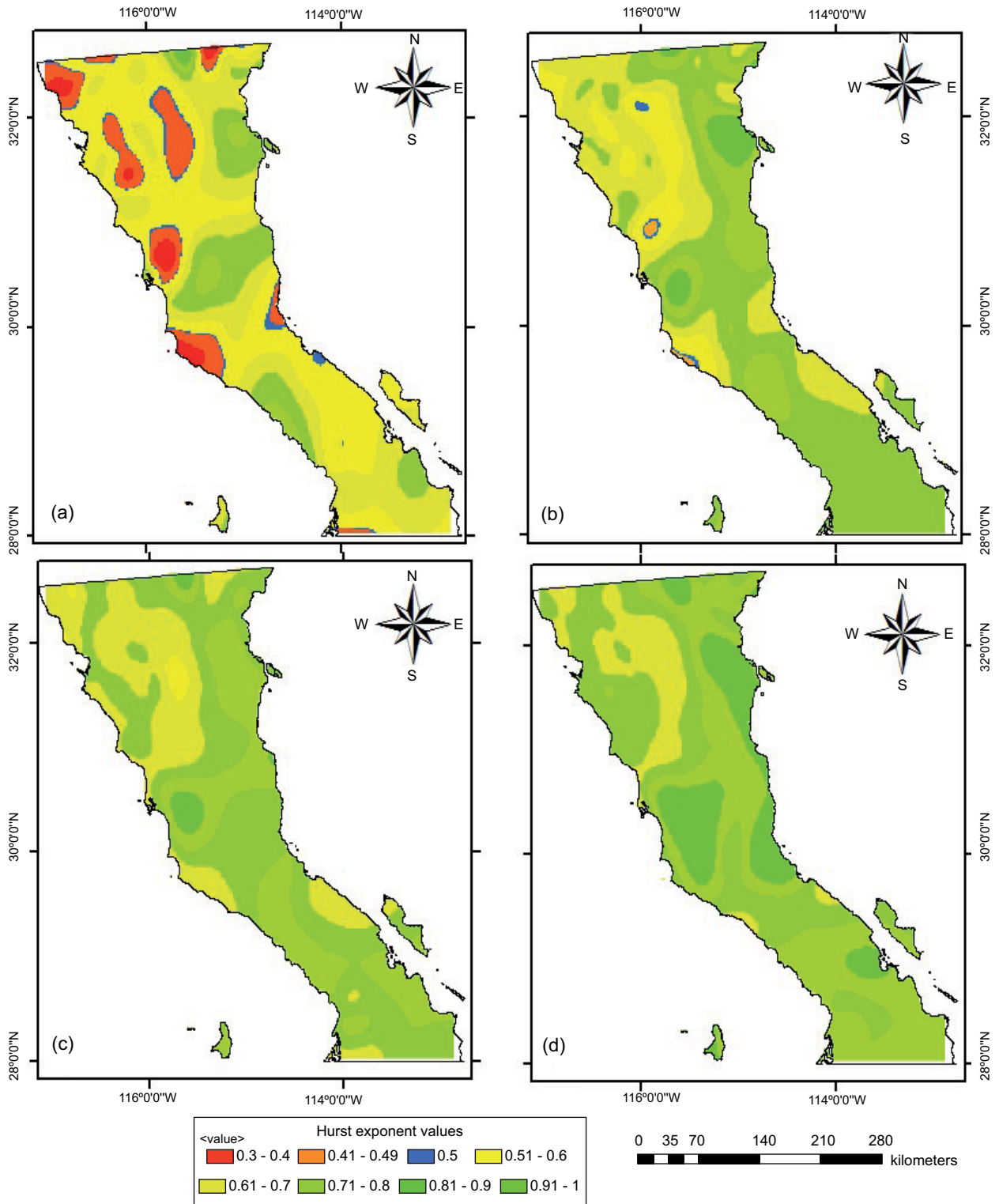


Fig. 3. Spatial and temporal variation from the Hurst exponent at different time scales. (a) Complete time series, (b) 25 yrs, (c) 10 yrs, (d) 5 yrs.

Table I. Average Hurst exponent results for climatological stations in Baja California sorted by type of climate

No.	Climatological station	Köppen climate classification	Latitude	Longitude	Average Hurst exponent for daily rainfall events (complete time series)
2001	Agua Caliente	BSks climate: cold	32.107	-116.454	0.51
2003	Bataquez	semiarid Mediterranean.	32.551	-115.069	0.61
2005	Boquilla de Santa Rosa I	Rainfall during winters	32.022	-116.777	0.54
2008	Colonia Guerrero		30.717	-115.983	0.53
2024	El Testerazo		32.296	-116.534	0.65
2029	La Providencia		30.969	-116.157	0.57
2035	Ojos Negros		31.912	-116.265	0.5
2036	Olivares Mexicanos		32.049	-116.681	0.53
2038	Presa Rodríguez		32.447	-116.908	0.45
2055	San Telmo		30.95	-116.1	0.55
2056	San Vicente		31.329	-116.248	0.48
2060	Santa Cruz		30.879	-115.628	0.52
2064	Santo Domingo		31.633	-116.377	0.58
2068	Tijuana		32.525	-117.042	0.49
2069	Valle de las Palmas		32.37	-116.654	0.48
2071	Colonia valle de la trinidad		31.356	-115.696	0.51
2079	El Alamar		31.836	-116.204	0.54
2089	Ejido Emilio López Zamora		31.104	-116.168	0.68
2091	Ejido Ignacio López Ray		31.288	-116.264	0.55
2092	Ejido San Matías		31.331	-115.544	0.56
2096	La Calentura		31.27	-116.037	0.59
2104	El Ciprés		31.79	-116.588	0.59
2106	Maneadero		31.696	-116.573	0.57
2108	Punta Banda		31.714	-116.666	0.59
2110	Guayaquil		29.967	-115.097	0.65
2118	Valle San Rafael		31.919	-116.234	0.54
2121	El Hongo		32.516	-116.303	0.52
2124	El Carrizo II		32.491	-116.684	0.53
2152	Ejido J. Maria del Pino		32.373	-116.068	0.62
2153	Ejido Uruapan		31.619	-116.455	0.61
2012	Ejido J. María Morelos	BWk(x') climate: cold arid	28.3	-114.026	0.65
2109	Santa Rosalita	desert. Rainfall all year	28.668	-114.237	0.69
2009	Colonia Juárez	BW(h')(x') climate: hot	32.299	-115.016	0.61
2011	Delta	and arid, sunny and dry.	32.353	-115.189	0.65
2016	El barril	Rainfall all year	28.302	-112.878	0.61
2020	El mayor		32.127	-115.278	0.69
2033	Mexicali (dge)		32.663	-115.468	0.57
2034	Mexicali (smn)		32.55	-115.467	0.6
2037	Presa Morelos		32.715	-114.729	0.61
2046	San Felipe		31.028	-114.835	0.66
2107	Percebú		30.886	-114.779	0.78
2139	Colonia Rodríguez		32.419	-115.036	0.73
2140	Colonia Zaragoza		32.61	-115.531	0.86
2141	Compuerta Benassini		32.57	-115.111	0.63
2145	Rancho Williams		32.624	-114.878	0.61
2154	Colonia zacatecas		32.06	-115.059	0.71

Table I. Average Hurst exponent results for climatological stations in Baja California sorted by type of climate

No.	Climatological station	Köppen climate classification	Latitude	Longitude	Average Hurst exponent for daily rainfall events (complete time series)
2002	Bahía de los Ángeles	BWh(x') climate:	28.604	-113.556	0.65
2006	Chapala	semicalid and arid.	29.488	-114.364	0.57
2059	Santa Clara	Rainfall all year	31.081	-115.286	0.58
2061	Santa Gertrudis		28.075	-113.092	0.62
2072	Presa Emilio López Zamora		31.896	-115.597	0.47
2093	Ejido Valle de la Trinidad		32.356	-115.749	0.57
2099	Rancho los Algodones		30.781	-115.175	0.74
2101	El Centinela		32.575	-115.742	0.81
2102	La Ventana		31.44	-115.054	0.71
2137	Colonia Mariana		32.259	-115.322	0.65
2146	Colonia San Pedro Mártir		31.038	-115.204	0.6
2151	Agua de Chale		30.638	-114.75	0.68
2023	El Socorro	BWks climate: cold and	30.321	-115.821	0.59
2031	La Rumorosa	arid. Rainfall during	32.549	-116.046	0.6
2032	Las Escobas	winters	30.579	-115.938	0.51
2043	San Agustín		29.938	-114.967	0.57
2063	Santa María del Mar		30.402	-115.888	0.54
2086	Ejido Jacume		32.591	-116.192	0.58
2111	Ejido Nueva Baja California		30.517	-115.931	0.62
2015	El Arco	BWhs climate: hot and arid,	28.029	-113.396	0.59
2022	El Rosario	semicalid. Rainfall during	30.059	-115.723	0.59
2027	Isla Cedros	winters	28.135	-115.175	0.71
2039	Punta Prieta		29.158	-114.146	0.57
2040	Rancho Alegre		28.229	-113.755	0.59
2041	Nuevo Rosarito		28.634	-114.017	0.58
2044	San Borja		28.735	-113.753	0.57
2051	San Luis Baja California		29.727	-114.711	0.62
2053	San Miguel		28.583	-113.95	0.62
2058	Santa Catarina Sur		29.722	-115.13	0.54
2084	El Progreso		29.968	-115.191	0.6
2085	San Regis		28.597	-113.755	0.59
2120	Ejido México		31.072	-116.206	0.64
2144	Ensenada Blanca		28.411	-113.864	0.69
2004	Ignacio Zaragoza	Cs climate: Mediterranean.	32.195	-116.486	0.54
2014	El Álamo	Rainfall during winters	31.593	-116.054	0.52
2019	El Compadre		32.338	-116.254	0.58
2021	El Pinal		32.183	-116.292	0.55
2045	San Carlos		31.785	-116.464	0.55
2049	San Juan de Dios del Norte		32.132	-116.165	0.52
2057	Santa Catarina Norte		31.657	-115.824	0.51
2065	Santo Tomás		31.792	-116.406	0.47
2088	Ejido Heroes de la Independencia		31.61	-115.938	0.61
2114	Ejido Carmen Serdán		32.244	-116.584	0.62
2050	San Juan de Dios del Sur	BSok(x') climate: cold semiarid. Rainfall all year	30.184	-115.137	0.69

Table II. Averaged Hurst exponent results for climatological stations in Baja California for all time scales for daily rainfall events

No.	Climatological station	Elevation (masl)	Average annual rainfall (mm yr <sup>-1</sup> )	Average annual temperature (°C)	Average Hurst exponent for the different time scales			
					Complete time series	25 yrs	10 yrs	5 yrs
2001	Agua Caliente	400	272.76	12.68	0.51	0.6	0.66	0.68
2002	Bahía de los Ángeles	4	67.31	21.98	0.65	0.74	0.79	0.81
2003	Bataquez	23	72.49	20.02	0.61	0.74	0.78	0.82
2004	Ignacio Zaragoza	540	297.63	12.21	0.54	0.62	0.69	0.73
2005	Boquilla Santa Rosa de L.	250	264.70	13.22	0.54	0.64	0.64	0.65
2006	Chapala	660	115.16	19.59	0.57	0.7	0.71	0.75
2008	Colonia Guerrero	30	159.04	15.34	0.53	0.61	0.67	0.71
2009	Colonia Juárez	17	59.73	19.01	0.61	0.68	0.78	0.79
2011	Delta	12	46.58	19.76	0.65	0.72	0.77	0.8
2012	Ejido J. María Morelos	20	62.74	15.53	0.65	0.77	0.79	0.85
2014	El Álamo	1115	268.82	13.66	0.52	0.6	0.66	0.72
2015	El Arco	288	102.75	17.62	0.59	0.74	0.78	0.86
2016	El Barril	50	81.31	24.12	0.61	0.76	0.78	0.85
2019	El Compadre	1110	308.55	18.84	0.58	0.68	0.63	0.69
2020	El Mayor	15	56.16	17.74	0.69	0.8	0.83	0.89
2021	El Pinal	1320	453.80	9.22	0.55	0.78	0.64	0.7
2022	El Rosario	40	168.59	16.78	0.59	0.72	0.76	0.81
2023	El Socorro	26	106.09	17.11	0.59	0.79	0.8	0.84
2024	El Testerazo	380	240.58	11.72	0.65	0.72	0.76	0.76
2027	Isla Cedros	3	62.73	19.74	0.71	0.81	0.84	0.87
2029	La Providencia	40	257.25	13.93	0.57	0.72	0.73	0.78
2031	La Rumorosa	1232	135.59	14.7	0.6	0.73	0.73	0.79
2032	Las Escobas	30	134.61	15.03	0.51	0.7	0.75	0.8
2033	Mexicali (DGE)	3	73.93	18.8	0.57	0.76	0.75	0.81
2034	Mexicali (SMN)	3	73.54	20.24	0.6	0.72	0.77	0.88
2035	Ojos Negros	680	226.76	12.73	0.5	0.61	0.66	0.69
2036	Olivares Mexicanos	340	279.97	14.46	0.53	0.68	0.7	0.76
2037	Presa Morelos	40	62.43	17.83	0.61	0.66	0.74	0.82
2038	Presa Rodríguez	120	232.25	14.63	0.45	0.62	0.65	0.7
2039	Punta Prieta	325	89.93	16.47	0.57	0.74	0.76	0.84
2040	Rancho Alegre	120	120.32	15.83	0.59	0.75	0.75	0.82
2041	Nuevo Rosarito	20	110.30	16.84	0.58	0.75	0.74	0.79
2043	San Agustín	552	111.09	17.13	0.57	0.75	0.76	0.81
2044	San Borja	445	104.99	18.03	0.57	0.73	0.76	0.85
2045	San Carlos	164	263.38	15.19	0.55	0.68	0.69	0.75
2046	San Felipe	10	64.96	22.5	0.66	0.84	0.86	0.94
2049	San Juan de Dios del Norte	1280	362.93	12.09	0.52	0.58	0.61	0.65
2050	San Juan de Dios del Sur	600	120.74	16.7	0.69	0.73	0.76	0.8
2051	San Luis Baja California	480	92.75	17.82	0.62	0.81	0.83	0.89
2053	San Miguel	440	124.93	19.44	0.62	0.71	0.7	0.77
2055	San Telmo	60	192.05	13.8	0.55	0.65	0.73	0.76
2056	San Vicente	110	211.76	13.21	0.48	0.65	0.73	0.74
2057	Santa Catarina Norte	1150	248.74	14.53	0.51	0.6	0.62	0.66
2058	Santa Catarina Sur	317	137.61	16.38	0.54	0.71	0.73	0.79
2059	Santa Clara	410	128.24	18.84	0.58	0.69	0.73	0.8
2060	Santa Cruz	980	265.14	15.57	0.52	0.63	0.66	0.71
2061	Santa Gertrudis	400	105.45	18.06	0.62	0.72	0.75	0.84

Table II. Averaged Hurst exponent results for climatological stations in Baja California for all time scales for daily rainfall events

No.	Climatological station	Elevation (masl)	Average annual rainfall (mm yr <sup>-1</sup> )	Average annual temperature (°C)	Average Hurst exponent for the different time scales			
					Complete time series	25 yrs	10 yrs	5 yrs
2063	Santa María del Mar	28	160.65	14.95	0.54	0.71	0.73	0.79
2064	Santo Domingo	250	211.54	14.06	0.58	0.72	0.74	0.79
2065	Santo Tomás	180	262.63	16.43	0.47	0.62	0.65	0.67
2068	Tijuana	20	220.40	15.22	0.49	0.62	0.66	0.72
2069	Valle de las Palmas	280	206.94	12.74	0.48	0.63	0.69	0.72
2071	Colonia Valle de la Trinidad	740	204.73	10.59	0.51	0.59	0.62	0.67
2072	Presa Emilio López Zamora	43	248.41	14.58	0.47	0.64	0.66	0.69
2079	El Alamar	710	264.09	12.8	0.54	0.63	0.68	0.69
2084	El Progreso	517	135.61	17.64	0.6	0.73	0.76	0.83
2085	San Regis	495	132.94	17.97	0.59	0.73	0.73	0.78
2086	Ejido Jacume	860	214.49	13.24	0.58	0.67	0.72	0.74
2088	Ejido Héroes de la Independencia	1000	263.63	14.08	0.61	0.71	0.72	0.75
2089	Ejido Emilio López Zamora	180	187.23	14	0.68	0.75	0.75	0.78
2091	Ejido Ignacio López Ray	170	269.95	11.88	0.55	0.67	0.69	0.74
2092	Ejido San Matías	968	214.29	15.95	0.56	0.63	0.67	0.73
2093	Ejido Valle de la Trinidad	780	231.19	11.6	0.57	0.71	0.74	0.79
2096	La Calentura	210	209.38	14.27	0.59	0.69	0.72	0.77
2099	Rancho los Algodones	460	72.87	19.22	0.74	0.78	0.8	0.87
2101	El Centinela	50	46.13	20.7	0.81	0.9	0.88	0.93
2102	La Ventana	16	36.33	21.3	0.71	0.88	0.88	0.92
2104	El Ciprés	8	202.84	15.25	0.59	0.7	0.72	0.74
2106	Maneadero	50	202.03	15.28	0.57	0.69	0.73	0.73
2107	Percebú	4	44.09	19.12	0.78	0.87	0.9	0.92
2108	Punta Banda	15	260.61	15.13	0.59	0.7	0.72	0.76
2109	Santa Rosalita	8	136.02	16.64	0.69	0.78	0.82	0.87
2110	Guayaquil	530	123.51	17	0.65	0.8	0.77	0.72
2111	Ejido Nueva Baja California	17	139.68	14.13	0.62	0.72	0.74	0.77
2114	Ejido Carmen Serdán	560	234.56	11.57	0.62	0.72	0.74	0.77
2118	Valle San Rafael	721	218.41	12.45	0.54	0.66	0.69	0.71
2120	Ejido México	75	176.97	13.61	0.64	0.71	0.75	0.78
2121	El Hongo	960	291.13	12.55	0.52	0.61	0.63	0.67
2124	El Carrizo II	300	233.74	13.59	0.53	0.63	0.65	0.68
2137	Colonia Mariana	9	57.61	19.4	0.65	0.78	0.75	0.82
2139	Colonia Rodríguez	17	36.84	18	0.73	0.88	0.82	0.9
2140	Colonia Zaragoza	8	65.17	12.43	0.86	0.82	0.88	0.94
2141	Compuerta Benassini	20	55.11	17.9	0.63	0.8	0.75	0.84
2144	Ensenada Blanca	10	89.08	19.7	0.69	0.75	0.82	0.84
2145	Rancho Williams	29	63.06	20.57	0.61	0.77	0.73	0.83
2146	Colonia San Pedro Mártir	416	106.32	16.19	0.6	0.75	0.74	0.81
2151	Agua de Chale	5	53.13	22.59	0.68	0.83	0.82	0.88
2152	Ejido J. María del Pino	1380	273.63	8.7	0.62	0.74	0.72	0.75
2153	Ejido Uruapan	195	288.55	13.9	0.61	0.7	0.72	0.75
2154	Colonia Zacatecas	12	53.55	18.46	0.71	0.81	0.8	0.87

warm conditions with the same rainfall regime  $BW(h')(x')$  cover the state of Baja California from north to south, exhibiting a high variability in the  $H_u$  value. The region comprising  $BWh(x')$  and  $BW(h')(x')$  climates is delimited by the geographical coordinates  $32.716^\circ$  N,  $114.719^\circ$  W, and  $29.943^\circ$  N,  $114.98^\circ$  W, where the obtained  $H_u$  values vary from 0.62 to 0.88, meaning there is a persistent behavior. Whereas, in the region limited by  $29.943^\circ$  N,  $114.963^\circ$  W, and  $28.743^\circ$  N,  $113.745^\circ$  W,  $H_u$  values for the climates in consideration vary from 0.5 to 0.58, which indicates a tendency to random behavior. An anti-persistent behavior in the rainfall series can hinder the prediction of a new rainfall event. The time of the year that does not present meaningful rainfall events can be the responsible for the anti-persistent behavior in the series (Velásquez et al., 2013).

From Table II and Figure 2c, which shows the variation of altitudes in Baja California, it can be observed that the highest altitudes, corresponding to the Sierra Juárez and Sierra San Pedro Mártir, are located in the central area. Moreover, comparing this map with the maps for annual precipitation (Fig. 2a) and average daily temperature (Fig. 2b), it is evident that regions in the studied area with higher altitudes have lower values for average daily temperatures, as well as greater values for average annual rainfall, in contrast with areas with altitudes close to the sea level. According to Table II, two climatological stations, Delta and San Vicente, are considered in order to illustrate the previously mentioned behavior. The Delta station is located at 12 masl, while the San Vicente station is located at 1150 masl. In Figure 2 it may be seen that the average annual rainfall regime is very low in Delta ( $46.65 \text{ mm yr}^{-1}$ ) compared to San Vicente ( $248.7 \text{ mm yr}^{-1}$ ). Regarding average daily temperature, the stations Delta and San Vicente reported  $19.76$  and  $13.21^\circ\text{C}$ , respectively.

It can be established that in Baja California, the average annual rainfall has a direct relation with the physiographic and altitude variables. The average annual temperature has a proportional inverse correlation with the magnitude of the average annual rainfall.

Given the importance of assessing the fractal behavior of the daily rainfall series and analyzing the variability of the  $H_u$  at different time scales, an analysis was carried out considering the previously

mentioned time scales, which correspond to  $H_u$  values resulting from the analysis of the complete time series for rainfall daily events, as well as for the different time scales (25, 10, and 5 yrs).

Table II depicts the behavior of Hurst values for daily rainfall events at different time scales where reported. From the data analysis two main behavior patterns can be noticed for each of the time series regarding the analyzed variable: anti-persistent and persistent. Both of these behavior patterns will be discussed below.

According to Table II, the stations Presa Rodríguez, San Vicente, Tijuana, Valle de las Palmas, Presa Emilio López Zamora, and Santo Tomás, which are located in the northeast region of Baja California, presented the following  $H_u$  values: 0.45, 0.48, 0.49, 0.48, 0.47 and 0.47, respectively, i.e., they are anti-persistent in time. This means that rainfall events that take place in this region have a high probability of showing a positive increasing behavior, followed by a decreasing behavior in its record values and vice versa. According to Malamud and Turcotte (1999), an anti-persistent time series will have a stationary behavior in time; due to the increases and decreases that compensate each other, statistical moments are independent from the time series. Rehman (2009) establishes that, in the case of rainfall, an anti-persistent behavior indicates a lesser dependency in accordance with previously stated values.

Nevertheless, when the rainfall series in the previously mentioned stations were analyzed in 25-yr scales, the Hurst values were reported as follows: 0.62, 0.65, 0.62, 0.63, 0.64 and 0.62, respectively. These values indicate a persistent behavior in time, which means that if the rainfall series registers a positive increase, it is more likely that a positive increase will follow. This implies that each rainfall event has a degree of occurrence over future events or in its long-term behavioral memory.

From the analysis of the previously mentioned stations for 10- and 5-yr increases in the Hurst values, considering this are noticeable and show a persistent behavior through time, it can be found that the  $H_u$  increases while establishing shorter time scales.

Anti-persistent series kept a positive increase tendency with minor negative increases; thus, while considering shorter periods of time (25, 10, 5 yrs), it is reasonable that series start to behave in a more

persistent manner. This is due to the fact that the shorter the considered time scale, the greater the possibility to analyze a time period with a predominant behavior (which in this case is persistent); this could explain the increase in the Hurst values in the analyzed rainfall series.

Continuing with the analysis of the remaining 86 stations, and considering the established time scales, increases in the Hurst values are noticeable with values greater than 0.5, indicating they keep a persistent behavior tendency. This means that rainfall series are not stationary and moments are dependent on the time scale. Persistency is an indicator that present events not only influence the near future but they will also have an impact in the long term.

A geospatialization of the  $H_u$  values obtained at different time scales and reported on Table III, was carried out to allow the study of the spatial and temporal variability in Baja California (Fig. 3).

Three areas with different behavior regarding the  $H_u$  can be noticed in Figure 3a: an anti-persistent area, a random area, and a persistent area. However, when a 25-yrs time scale is considered, the anti-persistent and indefinite areas start to decrease, as shown in Fig. 3b. Considering the 10- and 5-yrs time scales, a persistent behavior is noticeable throughout Baja California, as shown in Figure 3c, d.

Figure 3 shows a persistent tendency in the time series of the analyzed periods; however, we were able to identify a gradual increase in the  $H_u$  when time series were segmented in periods. A possible explanation for this behavior is that non-segmented time series take into consideration all sudden changes expressed in terms of variable increase/decrease, which can influence the possible presence of anti-persistent behavior patterns. Nonetheless, when an analysis is carried out in segmented time series, there is a possibility that sudden changes cannot be noticed, which directly affects the persistence strength of the time series and causes a gradual increase in the  $H_u$  values; however, fractality prevails in the series.

Temporal behavior of rainfall time series may be regionalized in space in order to study its relationship with geographical and physiographical variables. Figure 4a shows that the relationship between annual rainfall and the  $H_u$  is fairly convincing ( $r = 0.63$ ); also, according to the slope of the fitting line, this has an inverse relationship, and in Figure 4b, the  $H_u$  of

Table III. Correlation matrix among geographic coordinates and fractal statistics.

	Longitude	Latitude	Altitude	$D_{rs}$	$H_u$	Average annual rainfall (mm yr <sup>-1</sup> )	Median	SD	Temperature
Longitude	1								
Latitude	-0.76	1							
Altitude	0.15	0.31	1						
$D_{rs}$	-0.40	0.11	0.31	1					
$H_u$	0.40	-0.11	-0.31	-1.00	1				
Average annual rainfall (mm yr <sup>-1</sup> )	-0.68	0.32	0.60	0.62	-0.63	1			
Median	-0.68	0.34	0.59	0.66	-0.66	0.99	1		
SD	-0.59	0.21	0.55	0.46	-0.46	0.92	0.87	1.0	
Temperature	0.66	-0.35	-0.47	-0.43	0.43	-0.77	-0.76	-0.75	1

$D_{rs}$ : fractal dimension,  $H_u$ : Hurst exponent; SD: standard deviation.

the time series is also moderately influenced by the annual temperature ( $r = 0.43$ ). The altitude effect on the  $H_u$  is weak ( $r = 0.31$ ), which is shown in Figure 4c. It might be expected that the altitude effect on the

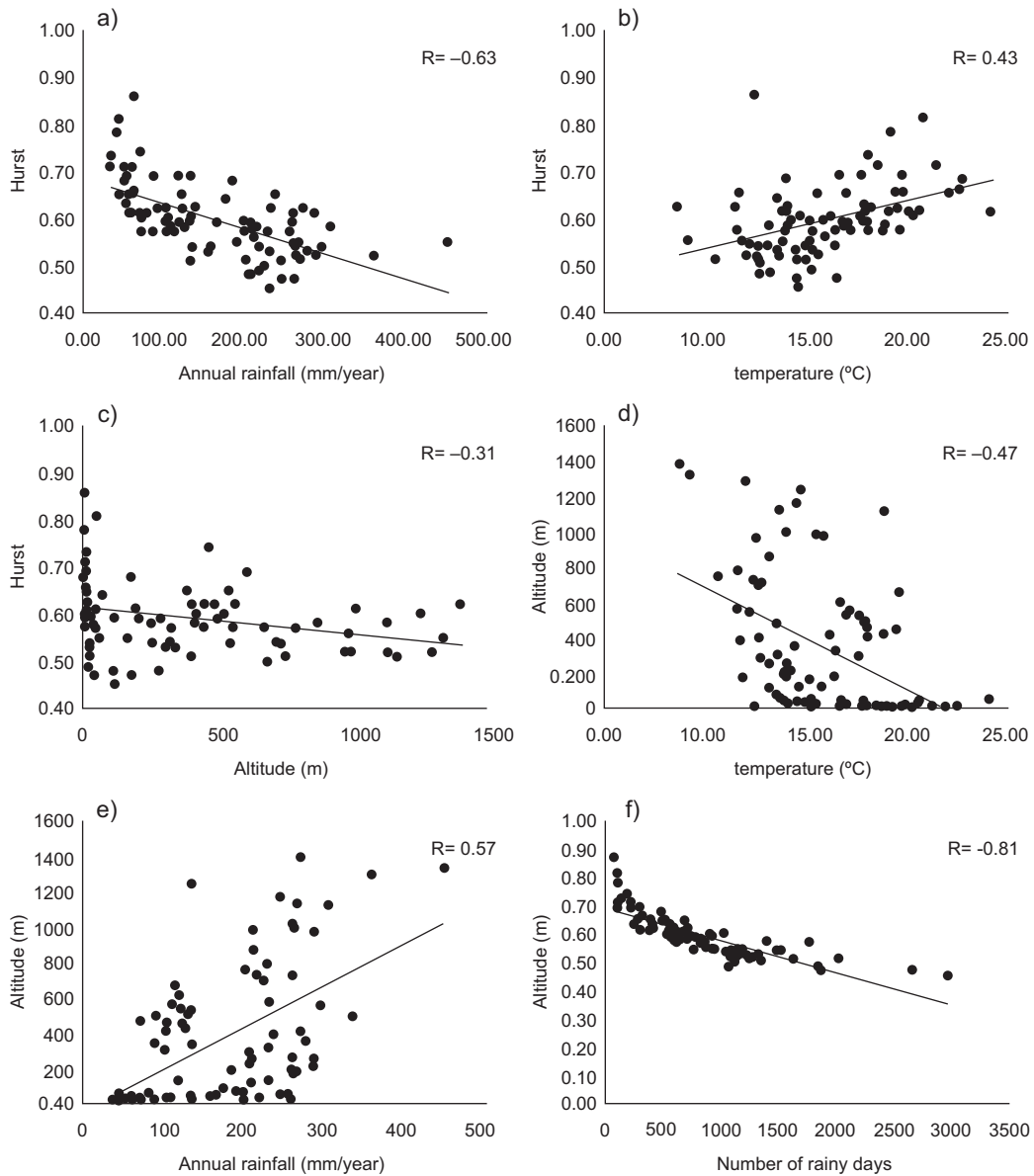


Fig. 4. Correlation analysis between the following variables: (a)  $H_u$  (complete time series) and average annual rainfall; (b)  $H_u$  (complete time series) and average annual temperature; (c)  $H_u$  (complete time series) and altitude ( $Z$ ); (d) altitude ( $Z$ ) and average annual temperature; (e) Elevation ( $Z$ ) and average annual rainfall; (f)  $H_u$  and days of precipitation.

dynamics of rainfall and temperature series would be especially strong. Actually, in Figure 4d the results show that there is a moderate relationship between temperature and altitude ( $r = -0.47$ ) and in Figure 4e the annual rainfall also seems to be associated with altitude ( $r = 0.60$ ). Another important parameter that determines the structural pattern in rainfall time series is the number of rainy days. In this research,

we found a strong correlation ( $r = 0.81$ ) between the number of rainy days and the  $H_u$  (Fig. 4f); these results are similar to those found by Velásquez et al. (2013).

It should be noted that for the semiarid to arid conditions of Baja California, we established a correlation matrix among geographic coordinates and fractal statistics, which is shown in Table III. High

correlations between fractal statistics mean a great interdependence, whereas these significant correlations between geographical coordinates and descriptive statistics suggest the strong influence of orography on rainfall (Magallanes et al. 2015), which is shown in Table III, where the relationship between  $H_u$  values and longitude is a significant positive correlation ( $r = 0.40$ ) and a significant negative correlation ( $r = -0.40$ ) between the fractal dimension and longitude. The present findings strongly suggest that the  $D_{rs}$  values of precipitation decrease as longitude increases, and  $H_u$  increases as longitude does. The output tells us that a very weak relationship between Hurst exponent values and latitude is  $-0.11$  for this data set. The relationship is negative. As latitude increases, the  $H_u$  value rate decreases.

#### 4. Conclusions

Even though three methods (M DFA, box counting, and R/S) were utilized to calculate the  $H_u$  for each analyzed scale time, it is difficult to determine which of these methods is the most efficient; however, the R/S method has been reported as the most used one.

Registered daily rainfall series throughout Baja California can be characterized by using the  $H_u$ , having as a result a tendency to present a persistent behavior. Thus, when a positive increase is registered, it is more likely that the following increase will be positive as well.

The Hurst exponents obtained from the rainfall time series are a measure to show a degree of dependency to the series, and can also explain the spatial and temporal behavior of rainfall in Baja California. This study suggests that rainfall series which took place in climates such as BWk(x'), BW(h')(x'), BW h(x'), and BSok(x'), presented a persistent behavior in time, which is due to  $H_u$  values fluctuating between 0.57 and 0.86. On the other hand, rainfall series which took place in climates such as BSks, Cs, BWks, and BWhs, showed a persistent and anti-persistent behavior, which is due to  $H_u$  values ranging from 0.4 to 0.6.

The existence of a dependency between rainfall and temperature as climate variables in relation to altitude can be noticed. Regions with altitudes close to the sea level tend to register the highest temperature values, as well as the lowest average annual rainfall. It can be established that a proportional inverse

relation between altitude and temperature exists, as well as a proportional direct relation between altitude and rainfall.

Taking into account the  $H_u$  used in this research, a proportional inverse relation with altitude and rainfall can be noticed; in regions that are close to the sea level, high values can be reported; on the other hand, in regions where the average annual rainfall is high the analysis showed low values for the  $H_u$ . It can be confirmed that the  $H_u$  depends on the climatological conditions and physiographic characteristics of a specific region.

It can be found that the series persistency is stronger when shorter time scales (25, 10, 5 yrs in this research) are considered. The greater the number of time scales considered for analyzing rainfall series, the greater the possibility of understanding its behavior and tendencies.

By geospatializing the  $H_u$  of the rainfall series, its variability regarding different climates in Baja California was traced and made visible. Besides, it provided data for the rainfall spatial-temporal behavior on this region.

Finally, it can be confirmed that fractal theory provides information that allows analyzing the occurrence of a climatological variable, such as rainfall (in the case of this research). This provides a useful tool to study and mitigate climate change in a given region.

It is recommended to use the multifractal theory in future researches, having as main purpose the opportunity to study the scale invariability from a mathematical perspective and to describe the climatic variable behavior with potential laws which are characterized by its exponents.

Multifractal theory allows describing precipitation behavior through potential laws that are characterized by their own exponents. It also constitutes a valid tool for the conceptualization of possible precipitation changes over time.

#### Acknowledgments

We would like to thank the Secretaría de Educación Pública (Secretariat of Public Education), which made this research possible by financing the project "Metodología para el análisis multifractal de la temperatura y precipitación" (Methodology for temperature and rainfall multifractal analysis) through

its professional and academic development program (PROMEP).

## References

- Akbari A. and Friedel M., 2014. Forecasting conditional climate-change using a hybrid approach. *Environ. Modell. Softw.* 52, 83-97.  
DOI: 10.1016/j.envsoft.2013.10.009
- Amaro I.R., Demey J.R. and Macchiavelli R., 2004. Aplicación del análisis R/S de Hurst para estudiar las propiedades fractales de la precipitación en Venezuela. *Interciencia* 29, 617-620.
- Arizabalo R., González-Ávalos E. and Korvin G., 2015. Multifractal analysis of atmospheric sub-micron particle data. *Atmos. Res.* 154, 191-203.  
DOI: 10.1016/j.atmosres.2014.11.008
- Beran J., 1994. *Statistics for long-memory processes*. Chapman and Hall, New York, 315 pp. DOI: 10.1007/978-3-642-35512-7
- Breslin M.C. and Belward J.A., 1999. Fractal dimensions for rainfall time series. *Math. Comp. S.* 48, 437-446.  
DOI: 10.1016/S0378-4754(99)00023-3
- Brunsell N., 2010. A multiscale information theory approach to assess spatial-temporal variability of daily precipitation. *J. Hydrol.* 385, 165-172.  
DOI: 10.1016/j.jhydrol.2010.02.016
- Caballero R., Jewson S. and Brix A., 2002. Long memory in surface air temperature: detection, modeling, and application to weather derivative valuation. *Clim. Res.* 21, 127-140. DOI: 10.3354/cr021127
- Callaghan S. and Vilar E., 2007. Fractal generation of rain fields: Synthetic realisation for radio communications systems. *IET Microw. Antennas Propag.* 1, 1204-1211.  
DOI: 10.1049/iet-map:20060126
- Capecchi V., Crisci A., Melani S., Morabito M. and Politi P., 2012. Fractal characterization of rain-gauge networks and precipitations: An application in Central Italy. *Theor. Appl. Climatol.* 107, 541-546.  
DOI: 10.1007/s00704-011-0503-z
- Chang J. and Wang L., 1999. The application of fractal study in forecasting flood calamities in Wuzhou, Guangxi. *Chin. Geogr. Sci.* 9, 184-188.  
DOI: 10.1007/BF02791371
- Falconer K., 1990. *Fractal Geometry: Mathematical Foundations and Applications*. 2nd ed. John Wiley and Sons, West Sussex, England, 284 pp.  
DOI: 10.2307/2532125
- Fluegeman R.H. and Snow R., 1989. Fractal analysis of long-range paleoclimatic data: Oxygen isotope record of Pacific core V28-239. *Pure Appl. Geophys.* 131, 307-313. DOI: 10.1007/BF00874493
- Ge E. and Yee L., 2013. Detection of crossover time scales in multifractal detrended fluctuation analysis. *J. Geogr. Syst.* 15, 115-147. DOI: 10.1007/s10109-012-0169-9
- Gires A., Tchiguirinskaia I., Schertzer D. and Lovejoy S., 2012. Influence of the zero rainfall on the assessment of the multifractal parameters. *Adv. Water. Resour.* 45, 13-25. DOI: 10.1016/j.advwatres.2012.03.026
- Gires A., Tchiguirinskaia I., Schertzer D., Schellart A., Berne A. and Lovejoy S., 2014. Influence of small scale rainfall variability on standard comparison tools between radar and rain gauge data. *Atmos. Res.* 138, 125-138. DOI: 10.1016/j.atmosres.2013.11.008
- Gutiérrez J.M., Galván A. and Cofiño A.S. (2006). Chaos game characterization of temporal precipitation variability: Application to regionalization. *Fractals* 14, 87-99. DOI: 10.1142/S0218348X06003088
- Hazewinkel M., 2001. Spline interpolation. In: *Encyclopedia of Mathematics*. Springer.  
Available at: [https://www.encyclopediaofmath.org/index.php/Spline\\_interpolation](https://www.encyclopediaofmath.org/index.php/Spline_interpolation).
- Huai-Hsien H., Puente C.E., Cortis A. and Fernández J.L., 2013. An effective inversion strategy for fractal-multifractal encoding of a storm in Boston. *J. Hydrol.* 496, 205-216. DOI: 10.1016/j.jhydrol.2013.05.015
- Hurst H.E., 1951. Long-term storage capacity of reservoirs. *Trans. Amer. Soc. Civil Eng.* 116, 770-880.
- Hurst H.E., 1956. Methods of using long-term storage in reservoirs. *P. I. Civil Eng.* 1, 516-543.  
DOI: 10.1680/iicep.1956.11503
- Kalauzi A., Cukic M., Millan H., Bonafoni S. and Biondi R., 2009. Comparison of fractal dimension oscillations and trends of rainfall data from Pastaza province, Ecuador and Veneto, Italy. *Atmos. Res.* 93, 673-679.  
DOI: 10.1016/j.atmosres.2009.02.007
- Kantelhardt J.W., Zschiegner S.A., Koscielny-Bunde E., Havlin S., Bunde A. and Stanley H.E., 2002. Multifractal detrended fluctuation analysis of nonstationary time series. *Physica A* 316, 87-114.  
DOI: 10.1016/S0378-4371(02)01383-3
- Köppen W., 1918. Klassifikation der klimate nach temperatur, niederschlag und jahresablauf (Classification of climates according to temperature, precipitation and seasonal cycle). *Petermann Geogr. Mitt.* 64, 193-203, 243-248.

- López-Lambraño A., Carrillo-Yee E., Fuente C., López-Ramos A. and López-Lambraño M., 2017. Una revisión de los métodos para estimar el exponente de Hurst y la dimensión fractal en series de precipitación y temperatura. *Revista Mexicana de Física* 63, 244-267
- Lovejoy S. and Mandelbrot B., 1984. Fractal properties of rain, and a fractal model. *Tellus*, 37A, 209-232.  
DOI: 10.1111/j.1600-0870.1985.tb00423.x
- Lovejoy S., Schertzer D. and Tsonis A.A., 1987. Functional box-counting and multiple elliptical dimensions in rain. *Science* 235, 1036-1038.  
DOI: 10.1126/science.235.4792.1036
- Magallanes R.M., Valdez R.D., Méndez S.J., Moreno A., Medina G. and Blanco F., 2015. Fractal analysis of monthly evaporation and precipitation time series at central Mexico. *Terra Latinoamericana* 33, 221-231.
- Malamud B.D. and Turcotte D.L., 1999. Self-affine time series: measures of weak and strong persistence. *J. Stat. Plan.* 80, 173-196.  
DOI: 10.1016/S0378-3758(98)00249-3
- Mandelbrot B.B., 1967. How long is the coast of Britain? Statistical self-similarity and fractional dimension. *Science* 156, 636-638.  
DOI: 10.1126/science.156.3775.636
- Mandelbrot B.B., 1972. Statistical methodology for non-periodic cycles: from the covariance to R/S analysis. *Ann. Econ. Soc. Meas.* 1, 259-290.
- Mazzarella A., 1999. Multifractal Dynamic Rainfall Processes in Italy. *Theor. Appl. Climatol.* 63(1-2), 73-78.  
DOI: 10.1007/s007040050093
- Millan H., Kalauzi A., Llerena G., Sucoshañay J. and Piedra D., 2008. Climatic trends in the Amazonian area of Ecuador: Classical and multifractal analyses. *Atmos. Res.* 88, 355-366.  
DOI: 10.1016/j.atmosres.2007.11.030
- Millan H., Kalauzi A., Cukic M. and Biondi R., 2010. Nonlinear dynamics of meteorological variables: Multifractality and chaotic invariants in daily records from Pastaza, Ecuador. *Theor. Appl. Climatol.* 102, 75-85. DOI: 10.1007/s00704-009-0242-6
- Millan H., Rodriguez J., Ghanbarian-Alavijeh B., Biondi R. and Llerena G., 2011. Temporal complexity of daily precipitation records from different atmospheric environments: Chaotic and Lévy stable parameters. *Atmos. Res.* 101, 879-892.  
DOI: 10.1016/j.atmosres.2011.05.021
- Movahed S., Jafari G., Ghasemi F., Rahvar S. and Rahimi M., 2006. Multifractal detrended fluctuation analysis of sunspot time series. *J. Stat. Mech.* P02003, 1-17.  
DOI: 10.1088/1742-5468/2006/02/P02003
- Nunes S., Romani L., Avila A., Traina C. Jr, de Sousa E.P.M. and Traina A.J.M., 2011. Fractal-based analysis to identify trend changes in multiple climate time series. *Journal of Information and Data Management* 2, 51-57.
- Oñate J.J., 1997. Fractal analysis of climatic data: Annual precipitation records in Spain. *Theor. Appl. Climatol.* 56, 83-87. DOI: 10.1007/BF00863785
- Pathirana A., Heath S. and Musiak K., 2001. Scaling rainfall series with a multifractal model. *J Hydr. Eng.* 45, 295-300.  
DOI: 10.2208/prohe.45.295
- Pavlopuolos H. and Krajewski W., 2014. A diagnostic study of spectral multiscaling on spatio-temporal accumulations of rainfall fields based on radar measurements over Iowa. *Adv. Water. R.* 74, 258-278.  
DOI: 10.1016/j.advwatres.2014.10.001
- Peñate I., Martín-González J.M., Rodríguez G. and Cianca A., 2013. Scaling properties of rainfall and desert dust in the Canary Islands. *Nonlin. Processes Geophys.* 20, 1079-1094. DOI: 10.5194/npg-20-1079-2013
- Peters O., Hertlein C. and Christensen K., 2002. A complexity view of rainfall. *Phys. Rev. L.* 88, 1-4.  
DOI: 10.1103/PhysRevLett.88.018701
- Pinel J., Lovejoy S. and Schertzer D., 2014. The horizontal space-time scaling and cascade structure of the atmosphere and satellite radiances. *Atmos. Res.* 140-141, 95-114. DOI: 10.1016/j.atmosres.2013.11.022
- Rangarajan G. and Sant D., 2004. Fractal dimensional analysis of Indian climatic dynamics. *Chaos Sol. F.* 19, 285-291. DOI: 10.1016/S0960-0779(03)00042-0
- Rehman S. (2009). Study of Saudi Arabian climatic conditions using Hurst. *Chaos Sol. F.* 39, 499-509.  
DOI: 10.1016/j.chaos.2007.01.079
- Schertzer D., Tchiguirinskaia I., Lovejoy S. and Hubert P., 2010. No monsters, no miracles: In nonlinear sciences hydrology is not an outlier! *Hydrol. Sci. J.* 55, 965-979.  
DOI: 10.1080/02626667.2010.505173
- Selvam A.M., 2010. Universal inverse power law distribution for fractal Fluctuations in Dynamical Systems: Applications for predictability of inter-annual variability of Indian and USA region rainfall. *Cornell University Library* 1-28. DOI: 10.1007/s00024-016-1394-9
- Selvi T. and Selvaraj S., 2011. Fractal dimension analysis of northeast monsoon of Tamil Nadu. *Univ. J. Environ. Res. Technol.* 1, 219-221.

- Shi P., Qiao X., Chen X., Zhou M., Qu S., Ma X. and Zhang Z., 2014. Spatial distribution and temporal trends in daily and monthly precipitation concentration indices in the upper reaches of the Huai River, China. *Stoch. Environ. Res. Risk Assess.* 28, 201-212. DOI: 10.1007/s00477-013-0740-z
- Sirangelo B. and Ferrari E., 2014. Analysis of the spatial correlation structure exhibited by daily rainfall in Southern Italy. *Theor. Appl. Climatol.* 118, 203-209. DOI: 10.1007/s00704-013-1042-6
- Sivakumar B., 2000. A preliminary investigation on the scaling behaviour of rainfall observed in two different climates. *Hydrol. Sci. J.* 45, 203-219. DOI: 10.1080/02626660009492320
- Svanidze G.G., 1980. *Mathematical modeling of hydrologic series*. Water Resources Publications, Fort Collins, Colorado, 314 pp.
- Tao K. and Barros A., 2010. Using fractal downscaling of satellite precipitation products for hydrometeorological applications. *J. Atmos. Oceanic Technol.* 27, 409-427. DOI: 10.1175/2009JTECHA1219.1
- Troutman B.M. and Over T.M., 2001. River flow mass exponents with fractal channel networks and rainfall. *Adv. Water R.* 24, 967-989. DOI: 10.1016/S0309-1708(01)00031-8
- Turcotte D., 1994. Fractal theory and estimation of extreme floods. *J. Res. Natl. Inst. Stand. Technol.* 99, 377-389. DOI: 10.6028/jres.099.036
- Velásquez M.A., Medina G., Sánchez I., Oleschko K., Ruiz J.A. and Korvin G., 2013. Spatial variability of the Hurst exponent for the daily scale rainfall series in the state of Zacatecas, Mexico. *J. Appl. Meteorol. Climatol.* 52, 2771-2780. DOI: 10.1175/JAMC-D-13-0136.1
- Venugopal V., Foufola-Georgiou E. and Sapozhnikov V., 1999. Evidence of dynamic scaling in space-time rainfall. *J. Geophys. Res.* 104, 31599-31610. DOI: 10.1029/1999JD900437
- Verrier S., de Montera L., Barthes L. and C. Mallet, 2010. Multifractal analysis of African monsoon rain fields, taking into account the zero rain-rate problem. *J. Hydrol.* 389, 111-120. DOI: 10.1016/j.jhydrol.2010.05.035
- Xu J., Chen Y., Li W., Liu Z., Tang J. and Wei C., 2015. Understanding temporal and spatial complexity of precipitation distribution in Xinjiang, China. *Theor. Appl. Climatol.* 123, 321-333. DOI: 10.1007/s00704-014-1364-z
- Yan-Fang S., 2013. A review on the applications of wavelet transform in hydrology time series analysis. *Atmos. Res.* 122, 8-15. DOI: 10.1016/j.atmosres.2012.11.003
- Yuval and Broday D.M., 2010. Studying the time scale dependence of environmental variables predictability using fractal analysis. *Environ. Sci. Technol.* 44, 4629-4634. DOI: 10.1021/es903495q
- Zhang Q., Zhang J., Yan D. and Wang Y., 2013. Extreme precipitation events identified using detrended fluctuation analysis (DFA) in Anhui, China. *Theor. Appl. Climatol.* 117, 169-174. DOI: 10.1007/s00704-013-0986-x
- Zhou X., Persaud N. and Wang H., 2005. Periodicities and scaling parameters of daily rainfall. *Ecol. Model.* 182, 371-378. DOI: 10.1016/j.ecolmodel.2004.04.011